KSÜ Mühendislik Bilimleri Dergisi, 27(1), 2024
Araştırma Makalesi

KSU J Eng Sci, 27(1), 2024
Research Article

Kahramanmaras Sutcu Imam University
Journal of Engineering Sciences

Geliş Tarihi : 14.09.2023
Kabul Tarihi :31.10.2023

Received Date : 14.09.2023
Accepted Date : 31.10.2023

IMPROVING THE BEHAVIOR OF RC FRAMES BY USING LIGHTWEIGHT CONCRETE PANELS AND METALLIC ELEMENTS

HAFİF BETON PANEL VE METALİK ELEMAN KULLANILARAK BETONARME ÇERÇEVE DAVRANIŞININ İYİLEŞTİRİLMESİ

Hakan KOMAN[1] (ORCID: 0000-0002-7309-7718)

[1] İstanbul Aydın Üniversitesi, İnşaat Mühendisliği Bölümü, İstanbul, Türkiye

*Sorumlu Yazar / Corresponding Author: Hakan Koman hakankoman@aydin.edu.tr

ABSTRACT

In this study, the effect of two different wall systems which are composed of the structural lightweight concrete panel and metallic elements between the wall and frame on the behaviour of the RC frame is investigated numerically by using the Abaqus software. In the second type of wall system, a polyurethane-based binder was used between the wall and the RC beam. A quasi-static lateral loading was applied to 5 different full scale RC frames with and without walls, and frames were pushed 80mm laterally. In the worst case, the wall system carried 1.52 times the lateral load bare frame carried, whereas in the best case, the frame with the wall system carried 2.12 times the load bare frame carried. When thinner metallic elements were used, the elements yielded. This is promising for increasing damping in structures also. The second type of wall which interacts with the beam increased the initial lateral stiffness of the frame by 156% when compared with the bare frame. All frames conducted a ductile behavior and bare frame results are validated by comparing with previous study.

Keywords: Abaqus, RC frame, numerical analysis, polyurethane binder

ÖZET

Bu çalışmada, yapısal hafif beton panel ve duvar ile çerçeve arasındaki metalik elemanlardan oluşan iki farklı duvar sisteminin betonarme çerçeve davranışına etkisi Abaqus yazılımı kullanılarak sayısal olarak incelenmiştir. İkinci tip duvar sisteminde duvar ile betonarme kiriş arasında poliüretan esaslı bağlayıcı kullanılmıştır. Duvarlı ve duvarsız 5 farklı tam ölçekli betonarme çerçeveye yarı statik yanal yükleme uygulanmıştır ve çerçeveler yanal olarak 80 mm itilmiştir. En kötü durumda duvarlı sistem, çıplak çerçevenin taşıdığı yanal yükün 1.52 katını taşırken, en iyi durumda duvarlı çerçeve, çıplak çerçevenin 2.12 katını taşımıştır. Daha ince metalik elemanlar kullanıldığında elemanlar akmıştır. Bu aynı zamanda yapılarda sönümün arttırılması açısından da ümit vericidir. Kirişle etkileşime giren ikinci tip duvar, çerçevenin başlangıç yanal rijitliğini çıplak çerçeveye göre %156 oranında arttırmıştır. Tüm çerçeveler sünek davranış sergilemiştir ve çıplak çerçeve sonuçları önceki çalışmayla karşılaştırılarak modelin güvenilirliği doğrulanmıştır.

Anahtar Kelimeler: Abaqus, betonarme çerçeve, nümerik analiz, poliüretan bağlayıcı

ToCite: KOMAN, H., (2024). IMPROVING THE BEHAVIOR OF RC FRAMES BY USING LIGHTWEIGHT CONCRETE PANELS AND METALLIC ELEMENTS. *Kahramanmaraş Sütçü İmam Üniversitesi Mühendislik Bilimleri Dergisi*, 27(1), 105-120.

INTRODUCTION

Strong earthquakes affect structures and cause big damage around the globe. Northridge 1994, Kocaeli 1999, Kahramanmaraş, 2023 earthquakes can be counted as examples of catastrophic damage. It's widely known that Türkiye's building stock consists of problematic, nonductile, reinforced concrete (RC) buildings. The buildings constructed before 1999 are examples of problematic building stock. Also, the recent Kahramanmaraş earthquakes (7.8 magnitude in Pazarcık region and 7.5 magnitude in Ekinözü region) revealed that some of the relatively new buildings that were constructed after the acceptance of regulations in the Turkish Seismic Code (TSC) 2007 and 2018 had severe damage or collapsed.

Modern seismic design philosophy expressed in seismic codes relies on the ductility of structures. Most of the damage is expected to happen in the plastic hinges which will be formed at the ends of beams during strong ground motions. The strong column-weak beam principle in codes aims to provide the ideal collapse mechanism where plastic hinges will be formed at the ends of beams and the bottom of the first story's columns (Bai and Ou, 2012). That principle is one of the explanations for damage that happened in relatively new buildings also. In a preliminary assessment report of Kahramanmaraş earthquakes (Demir et al., 2023), it was stated that the highest ground acceleration of the earthquake experienced on February 6, 2023, was approximately 4-5 times greater than the ground acceleration determined by the Turkey Earthquake Hazard Map for a residential building in Kahramanmaraş region. That means damage was more than expected in the buildings which were built properly. Also, the second earthquake hit the damaged buildings where plastic deformations already occurred due to the previous earthquake, causing collapse.

These earthquakes revealed the importance of increasing the energy consumption capacity and lateral load capacity of the structures once again. New buildings can be designed with a guarantee for extra energy consumption capacity and existing buildings can be seismically retrofitted. However different kinds of seismic retrofitting strategies can be suitable for different kinds of buildings. In practice, adding RC walls to the structures is a popular method. This type of design for retrofitting existing buildings or for construction of the relatively new buildings can be considered to increase the lateral stiffness of the structure. However, this is a time consuming and relatively expensive process and often residents do not want to move away during the retrofitting process.

Another strategy is placing seismic dampers on the structures. In this strategy, the main purpose is to increase the energy consumed by the damping mechanism in structures and thus decrease the energy consumed due to the plastic deformation of structural elements. In a previous study, for the seismic retrofit project of a building in Istanbul, traditional retrofitting methods were compared with placing dampers inside the structures. For that purpose, a kind of hybrid damper that relies on the combined effects of friction forces and viscoelastic behavior was selected. To replace the dampers inside the RC frame, steel diagonals were used. According to the results of the analysis, in the structure without any dampers, 34 of the 124 columns were damaged beyond the "life safety" level and 37 columns were damaged beyond the "before collapse" performance level. In the structure with dampers, only 20 of the 124 columns were damaged beyond the "life safety" level, and no column was damaged in the region of "collapse" or "before collapse". In the structure with dampers, the damping ratio was increased to around 22-23% in X and Y directions and base shear decreased by 13.02% to 24.01%. However, in the structure where RC walls were added, base shear increased by 191% to 230% in two of the directions. It was concluded that the placement of dampers was an economical and alternative method for seismic retrofit purposes (Yıldırım et al., 2014).

In another study, metallic yielding dampers were selected for the analysis. A few kinds of metallic yielding dampers were described. Some dampers relied on shear deformations, on the other hand, others relied on flexural deformations to consume energy. In the analysis of RC buildings with placement of metallic yielding kind of dampers, it was concluded that the building response was decreased by 35%. In this study, dampers were replaced in RC buildings by using steel diagonals (Li et al., 2014).

In another study, steel honeycomb dampers which were used in the automobile industry were implemented to be used in RC buildings for seismic retrofitting process. Honeycomb dampers were placed in the frame between steel diagonals and RC beams. A 15 story RC structure was analyzed by using 7 earthquake records. It was concluded that the placement of dampers decreased the story drifts. When the base shears were compared after a pushover analysis, it was concluded that for the same lateral drift ratio of 0.02, the structure without dampers carried 1000kN lateral load whereas the structure with dampers increased its capacity to 2500kN. Honeycomb dampers not only increased the damping but also increased the stiffness of the system. (Naeem et al., 2015).

In the other study, analysis was performed with friction type of dampers. When the steel braces containing friction dampers were added to the existing frames, the lateral strength and stiffness increased, the moment loads on the columns decreased, but the column axial forces increased. Reinforced concrete walls are rigid in shear and are disadvantageous in using friction dampers as they cannot provide the required displacement. It was stated that the friction load that activates the friction dampers can be selected so that the structure can remain elastic in the expected effects such as wind and small ground movement (Nikam et al., 2014).

On the other hand, the neediness of using steel braces to place dampers inside frames can be problematic for architectural purposes. Because often walls are needed for the separation of rooms inside a structure. To overcome this problem, transforming infill walls into an energy dissipating system by using mortarless blocks were proposed in a previous study (Lin et al., 2016). Experiments showed that a mortarless masonry infill wall increases the energy consumption of the frame without increasing the stiffness of the frame when the frame is in the elastic stage. In the study, the density of the concrete blocks used in the wall is 2250kg/m3, and the compressive strength is 18.3MPa, to reflect the behavior of the mortarless plug-in brick. Its dimensions were 227x113x80mm. The friction coefficient was found to be 0.66 in the experiments (Lin et al., 2016). An axial pressure of 0.3MPa was applied to the reinforced concrete frame beam, representing the weight of the 3-storey residential building. A lateral displacement of 10mm was applied to the frame without wall, 16mm to the frame with mortarless wall, and 20mm to the conventional walled frame. (slip rate around 1%). Bricks made friction movement only with their own weight. For stiffness comparison, secant stiffnesses obtained from the maximum values at various displacements in the hysteresis plot were used. It is compared with the initial stiffness of the empty frame. While the conventional wall increased the initial stiffness of the frame by around 30 times, the wall without mortar increased the stiffness of the frame by about 2 times. According to this result, the mortarless masonry wall can be considered as an energy absorber mechanism. The maximum load carried by the empty frame was 18.05kN, and the energy consumption up to this load was 91.812kNmm, while the energy consumption of the conventional walled frame was 3.07kNmm up to this load. The energy consumption of the mortarless masonry frame was 147.32kNmm up to this load, which is 50 times that of the conventional walled frame (Lin et al., 2016).

Also, in Turkish Seismic Code 2018 (TSC2018), it's emphasized that the interaction of infill walls inside RC frames changes the behaviour of structures, and relative story drift controls are performed differently according to the interaction between frame and infill wall. If stiff joints are used between the wall and frame like using mortar binder, then more rigid RC elements are used in design.

In this study, a new type of wall system is considered. Structural lightweight concrete panels were considered as walls and the effect of placing metallic elements between the wall and RC frame was analyzed numerically. The application of a wall system is practical, so it can be used either in existing buildings for retrofitting purposes or in new building constructions. Two different types of lightweight concrete wall panels are considered. In the first type, the wall height and width were short enough that there was no interaction between the wall and the RC frame. In the second type of wall, the top of the wall interacts with the RC beam inside the frame, whereas, the width of the wall is short enough to cease the interaction between the wall panel and RC columns. Between wall panels and the RC frame, metallic elements are placed and they are considered to be anchored to the RC beam and wall. The thicknesses of elements between the wall and frame were considered to be different. Different thicknesses improved the energy consumption and stiffness of the frame at different levels. Also, the second type is reasonable to make the wall panel contribute to vertical load carrying. The interaction between the panel and RC beam increases the lateral stiffness more than the first type of wall. The reason for selecting a wall rather than steel diagonals is to eliminate the architectural problems mentioned before. Lightweight steel fibered concrete was selected to decrease the total weight and to eliminate the neediness of rebar workmanship. The stress analysis showed the wall can carry the loadings without damage at all. The RC frame used in a previous study (Zhai et al., 2016) was selected for modelling the frame to compare the results with experiments. However equivalent local steel and concrete materials were considered to be used in RC members to represent the structures in Türkiye. The proposed method is advantageous for increasing the stiffness, lateral load capacity, and energy consumption of RC frames with a practical application.

MATERIALS AND METHOD

Modelling of Concrete

The CDP (Concrete Damaged Plasticity) model in Abaqus was used to model the behavior of concrete. The CDP model is one of the theories to predict the plastic deformation state of a material under stress. In some of the failure

theories, the stress tensor is thought to be divided into two parts: the hydrostatic part and the deviatoric part. Von Mises's theory states that hydrostatic stresses can create elastic volume change, but in the hydrostatic stress part, no shear stresses were included. Unlike shear stresses, hydrostatic stresses cannot cause deformation. Therefore, only deforming stresses should be taken into account. For this purpose, it considers the second constant coefficient of the stress tensor (J_2) and suggests that if this constant coefficient exceeds a certain value, then permanent strain begins. J_2 can be seen in equation 1 (Koman, 2021). Here $\boldsymbol{\sigma}$ indicates normal stresses, τ indicates shear stresses.

$$J_2 = \frac{1}{6}\left[(\sigma_{xx}-\sigma_{yy})^2+(\sigma_{yy}-\sigma_{zz})^2+(\sigma_{xx}-\sigma_{zz})^2\right]+{\tau_{xy}}^2+{\tau_{xz}}^2+{\tau_{yz}}^2=r^2 \quad (1)$$

In the Drucker-Prager criterion, both the deforming deflection stress tensor as in the Von Mises strain criterion and the volume-changing hydrostatic pressure, which is not taken into account in the Von Mises criterion, are taken into account. It can be expressed as follows (Kuruşçu, 2012):

$$F(I_1,J_2)=\boldsymbol{\alpha} I_1+\sqrt{J_2}-K \quad (2)$$

In equation 2, I_1 is the first invariant of the stress tensor. J_2 is the second invariant of the deviatoric stress tensor, α and K are coefficients related to cohesion and internal frictional angle. The CDP model is a modification of the Drucker-Prager criterion. It uses the yield surface proposed by Lubliner et al., (1989) and includes modifications proposed in the literature that include differential evolution of tensile and compressive strength. According to the modifications, the yielding (permanent deformation) surface in the deviatoric plane does not have to be a circle and this surface is adjusted with the K parameter (Al Shaikh and Falah, 2014).

The stress-strain relationships for concrete were considered as shown in Figure 1 (Obadiat, 2011) and the d_c parameter (it shows the effects that degrade the elasticity of the concrete in compression) was assumed to be zero. The strain corresponding to the maximum stress is taken as $0.0022(\boldsymbol{\varepsilon_0})$ for C25 and the modulus of elasticity was taken as 31000MPa. The strength of C25 concrete (f_0) was taken as 30MPa because the cubic test result must be used in Abaqus. A previous study in the literature was used to determine the values in the stress-strain graph of concrete. The stress-strain graph was created according to Equation 3 taken from this study (Inclunet, 2016).

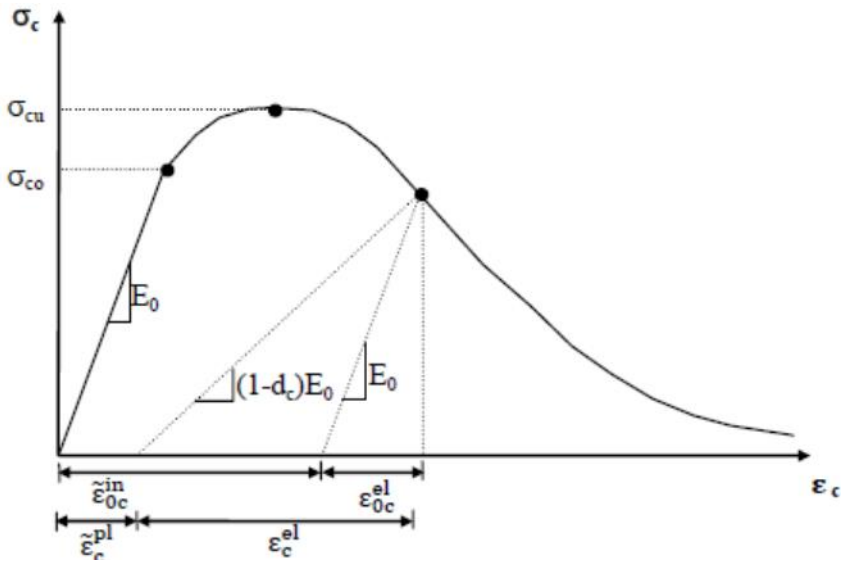

Figure 1. Stress-Strain Relationship of Concrete in Abaqus (Obadiat, 2011)

$$\frac{f}{f_0}=2.1\left(\frac{\varepsilon}{\varepsilon_0}\right)-1.33\left(\frac{\varepsilon}{\varepsilon_0}\right)^2+0.2\left(\frac{\varepsilon}{\varepsilon_0}\right)^3 \quad (3)$$

In equation 3, the cubic strength of concrete, f_0=30MPa, strain corresponding to maximum stress, ε_0=0,0022, maximum strain, ε_{max}=0.0035. In Abaqus, when defining materials, plastic deformation values are used, not the strain (ε) values. The tensile strength of concrete is defined by $0.7\sqrt{fck}$. Stress-strain behaviour in the tensile situation was considered to be linear until the strength of the material. Beyond that point, an exponential decrease was considered in the stress-strain graph. Again, the plastic deformation values were used and d_t parameter (it indicates the effects that degrade the elasticity of concrete in tension) was considered to be zero. For the CDP model in Abaqus, other parameters were needed. Dilation angle (the expansion angle in p-q plane), eccentricity, (the ratio between the

tensile strength and the compressive strength of the concrete), fbo/fco ratio (The ratio between the compressive strengths of concrete in two directional loading and unidirectional loading situation) was assumed as 38 degrees, 0.1, 1.16 respectively. These assumptions for parameters were used in a previous experimental and numerical study where numerical simulation gave approximate results to experimental results (Obadiat, 2011).

Modelling of Steel

Two kinds of steel were used in this study. Their mechanical properties were taken from a previous study (Koman, 2021) where mechanical properties of steel materials had been obtained by local producers' tests. For determining stress-strain curves, the approach of Turkish Seismic Code 2018 (for nonlinear analysis) was used in the previous study. The steel for longitudinal rebars had a strength of 491 MPa yield strength and 553MPa tensile strength. Its commercial name was B420C. The steel for stirrups had 277MPa yield strength and 387MPa tensile strength. Its commercial name was SAE steel. The behaviour of steel was assumed to be the same in tension and compression. The steel strain curves of steel materials can be seen in Figure 2. SAE steel is used for metallic elements also.

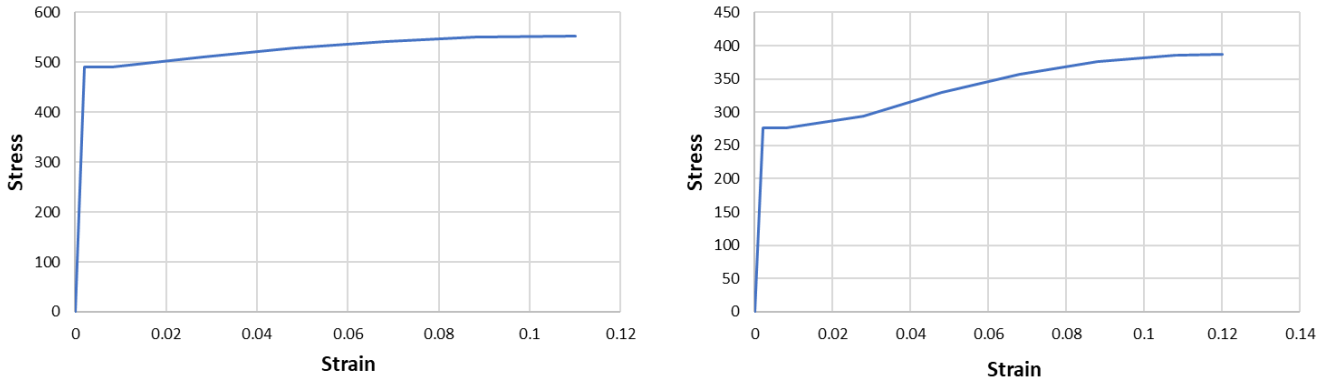

Figure 2. **a.** Stress-Strain Curve of B420C Steel **b.** Stress-Strain Curve of SAE Steel

Modelling of Lightweight Concrete

A steel fiber-reinforced lightweight concrete with superior strength properties was employed in the construction of the wall. This concrete, characterized by its high strength, was previously developed through an experimental investigation utilizing expanded clay aggregates. The concrete's specific properties were derived from a prior research study. In this earlier research, various concrete mixtures were formulated to assess the impact of steel fiber quantity on the concrete's compressive strength (Gao et al., 1997). The study concluded that the compressive strength of lightweight concrete could be altered based on factors such as the aspect ratio of the fibers and the volume of fibers used. The test results demonstrated the feasibility of producing lightweight concrete with an impressive compressive strength of 85.4MPa and a tensile strength of 11.8MPa. The density of the concrete measured 1966kg/m3. The study established the concrete's modulus of elasticity at 28000 MPa, and it introduced an equation for calculating this property. Additionally, the Poisson's ratio for this concrete was adopted as 0.16 (Gao et al., 1997)

Other parameters for the CDP model were assumed to be the same as ordinary concrete. Dilation angle, eccentricity, and fbo/fco ratio were assumed as 38 degrees, 0.1, 1.16 respectively. For the stress-strain relationships of the concrete, the Hognestad model was used. As previously mentioned, Abaqus requires the incorporation of plastic strains in the CDP model. Figure 3 illustrates the stress-strain relationships for the high-strength lightweight concrete containing steel fibers in compression. Figure 4 illustrates the stress-strain relationships in tension. The tensile stress behavior of concrete is assumed like an exponentially decreasing graph.

Modelling of Polymer Material

When employing the second type of wall panel, it interacts with the beam. In this area, a polymer binder known as "polymer pm" was selected. Polymer pm is a two-component polyurethane binder, consisting of two distinct components. Upon initial application, it takes on a fluid form but rapidly hardens within a few minutes after mixing with the other component. Once hardened, this binder exhibits rubber-like properties.

In a prior study (Kwicien, 2014), the comparison between epoxy and a polyurethane binder was conducted for seismic retrofitting of masonry structures using fiber-reinforced polymers (FRP). In this previous research, the Mooney Rivlin theory was chosen to model the behavior of the polymer material. The Mooney Rivlin theory is a suitable

approach for modeling hyperelastic materials, such as rubber, as the stress-strain relationship of hyperelastic materials is non-linear. Moreover, there is an increase in stress after experiencing significant strains, which classical theories cannot adequately explain. Instead, the theory relies on a strain energy function that characterizes the area under the stress-strain curve.

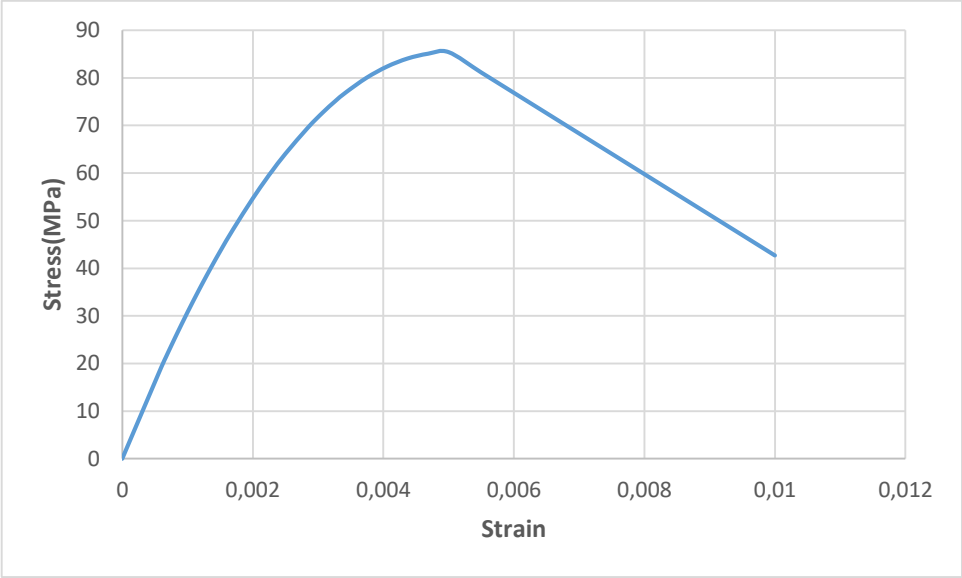

Figure 3. Hognestad Model for Stress Strain Relationship of Lightweight Concrete

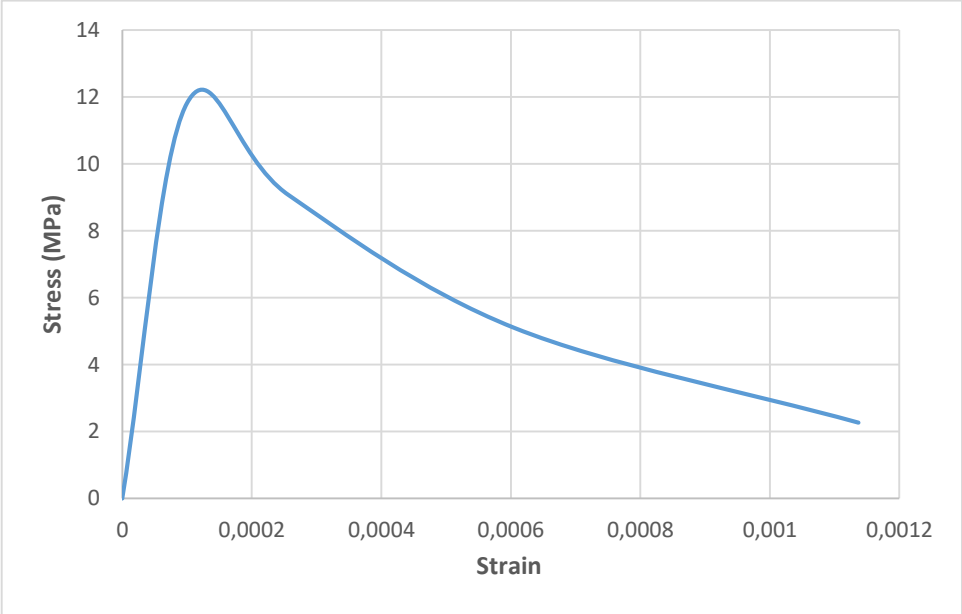

Figure 4. Stress-Strain Relationships of Lightweight Concrete in Tension

The equations for the Mooney Rivlin theory are detailed in equations (3-7), as described in the aforementioned prior study (Kwiecien, A., 2014):

$$W^{M-R} = C_{10}\left(\Delta^2 + \frac{2}{\Delta} - 3\right) + C_{01}\left(\frac{1}{\Delta^2} + 2\Delta - 3\right) \quad (3)$$

$$S_1 = \frac{F}{A_0} = \frac{dW^{M-R}}{d\Delta} = 2(C_{10}\left(\Delta - \frac{1}{\Delta^2}\right) + (C_{01}\left(1 - \frac{1}{\Delta^3}\right) = 2\left(1 - \frac{1}{\Delta^3}\right)(\Delta C_{10} + C_{01}) \quad (4)$$

$$E_0 = 3G_0 = 6(C_{10} + C_{01}) \quad (5)$$

$$G_0 = 2(C_{10} + C_{01}) \quad (6)$$

$$\Delta = \frac{L}{L_0} = \varepsilon + 1 \quad (7)$$

in this context, W^{M-R} represents the strain energy function for the hyperelastic material. S_1 denotes the stress, while E_0 represents the Young's modulus, and G_0 is the shear modulus. ε stands for the strain, L signifies the length after loading, and L_0 is the initial length. The coefficients C_{10} and C_{01} are specific to the Mooney-Rivlin Theory. C_{01} was determined to be -0.05, and C_{10} was calculated as 0.47, relying on experimental data obtained from a prior study (Ksiel, 2018).

Modelling of The Interaction Between Polymer and Other Materials

Surfaced based cohesive behavior is one method for modeling the interaction between binders and materials in Abaqus. Using the traction separation constitutive model, surface-based cohesive behavior makes it possible to model connections with interface thicknesses that are barely noticeable. The formulae for surface based cohesive behaviour are very similar to the formulae used for cohesive elements with traction separation. To describe the behavior of joints in tension and shear failure modes, traction separation laws are used. In Figure 5, traction separation is described. When the assembly is first loaded, the joint behaves linearly elastically, and Kn, Ks, and Kt express the stiffness of the joint. Following the peak traction value, the joint's plastic response begins. According to Figure 4, the maximum stress values are t_n^{max}, t_s^{max}, t_t^{max}, the separation values corresponding to the maximum stresses are δ_n^{max}, δ_s^{max}, δ_t^{max} respectively, and the separations at failure are δ_n^f, δ_s^f, δ_t^f (Abaqus Guide).

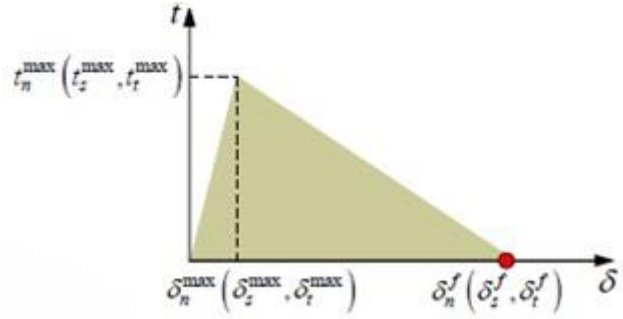

Figure 5. Traction Separation Laws (Abaqus Guide)

Damage initiation was determined using the maximum nominal stress criterion available in Abaqus. To characterize the behavior after joint failure, a Mohr-Coulomb shear sliding model was established with a friction coefficient of 0.66. Consequently, when the shear stress exceeds a critical threshold, the joint experiences sliding. The fracture energies of the joints were determined based on experimental results. In a previous study conducted by Viskovic et al. in 2017, experiments were conducted to ascertain these fracture energies. For flexible joints constructed with a polymer binder, the modified fracture energy was found to be 4.22 N/mm for failure mode mod 1 (tension) and 10.93 N/mm for failure mode mod 2 (shear). These values were utilized in the numerical analysis. Both the formulas used for cohesive elements with traction-separation behavior and those employed for surface-based cohesive behavior were found to be remarkably similar, as documented in the Abaqus manual. Consequently, the region beneath the traction-separation graph, commonly referred to as the fracture energy, was assumed to be constant. To capture mixed-mode behavior, the Benzeggagh-Kenane rule was applied in Abaqus. Previous research indicates that the Benzeggagh-Kenane mode is the optimal choice for capturing the critical mixed-mode fracture energy in cases where the critical fracture energies for second and third mode shear failures are equal. Furthermore, an exponent of 2 for the Benzeggagh-Kenane rule was selected by recommendations from the same study for brittle behavior (Abdulla et al., 2017).

Frame Properties and Loading Conditions

The frame properties were taken from a previous study where experimental and numerical analysis with Abaqus was performed (Zhai et al, 2016). That way, the results written here can be compared with the experimental and numerical results obtained previously. However, the steel and concrete materials were changed with the local equivalents. The difference between the strength of materials was in an acceptable range. In the previous study, the compressive strength of concrete used in Abaqus was 27.74MPa whereas here it was taken as 30MPa in Abaqus (cubic strength). Full scale single story RC frames were used for analysis. For the steel used in experimental and numerical analysis in the previous study, the yield and tensile strength of the material were 472MPa and 656MPa respectively whereas here, the yielding and tensile strength values were 491MPa, 553MPa respectively (steel for longitudinal rebars). In confinement rebars, in the previous study, a steel with a yielding strength of 308 MPa was used whereas in this study the yielding strength of the material was 277MPa as explained before.

The height of the columns was taken as 2600mm (measured till the bottom of the beam), and the bay length was 2800mm. Column cross section was assumed to be 350mm x350mm, beam cross section was assumed to be 350mm x 400 mm. The longitudinal rebars of the column were assumed to be 8ϕ16, and the longitudinal rebars for the beam were 4ϕ16. For confinement rebars of beams and columns ϕ8/100/150mm was used. The base of each column was assumed to be fixed support in numerical analysis, which was why no foundation beam was modelled separately. Axial forces of 700kN (5.71 MPa to column surface) were applied to the columns as a vertical loading. Later, a second specimen was prepared with a wall panel and metallic elements inside the frame. The properties and rebars of the RC frames which are taken from previous studies can be seen in Figure 6 (Zhai et al., 2016). All the measurements are given in mm. Figure 6 also shows the proposed wall system with polymer material.

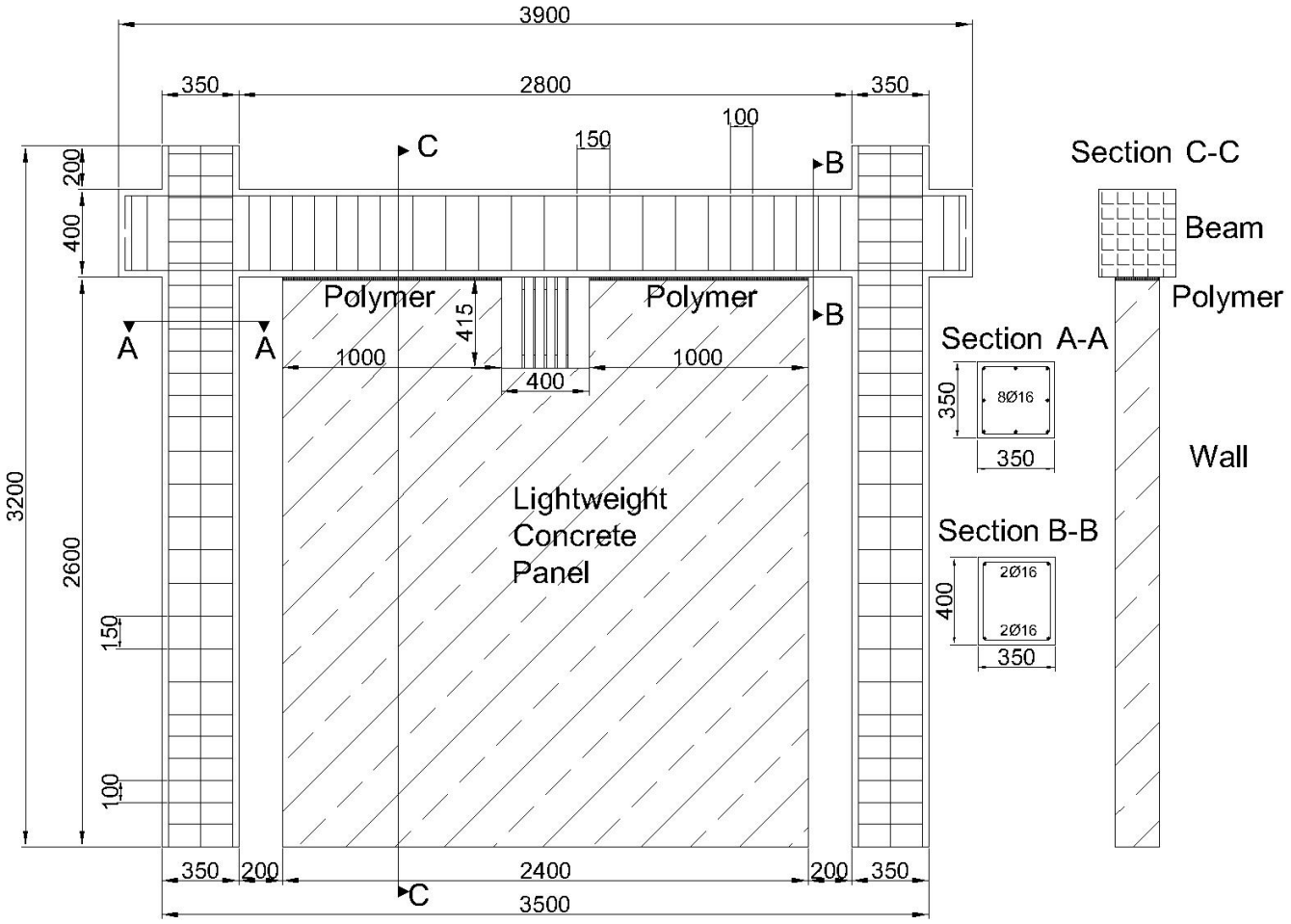

Figure 6. Dimensions of Frame with 2nd Type of Wall and Rebars of RC Frame

Two different kinds of walls were modelled to implement metallic elements inside the frames. In the first type of wall which is constructed by using structural lightweight concrete, the wall height and width were considered as 2185mm and 2400mm respectively. The metallic elements were replaced in the gap between the wall and the beam. In the second type of wall, the height was extended to 2585mm at the left and right regions of metallic elements. A polymer binder with a thickness of 15mm was implemented between the wall and frame. In this type of frame, compressive strut behaviour due to the application of the wall was expected. Therefore, an increase in the lateral stiffness of the frame was expected. This type of wall can be also useful for carrying vertical loads of the system if columns fail due to shear forces.

The metallic elements were considered as π-shaped elements as seen in Figure 7. Five steel elements with a height of 400mm, and width of 200mm were placed between walls and frames. The thickness of these elements was considered as 10mm in the first group of analysis where proposed wall types were compared with each other. Later a second group of analysis was conducted. In the second group of analysis metallic elements with 5mm and 3mm thicknesses were used. The cross-section of metallic elements can be seen in Figure 7. All of the measurements shown are given in mm.

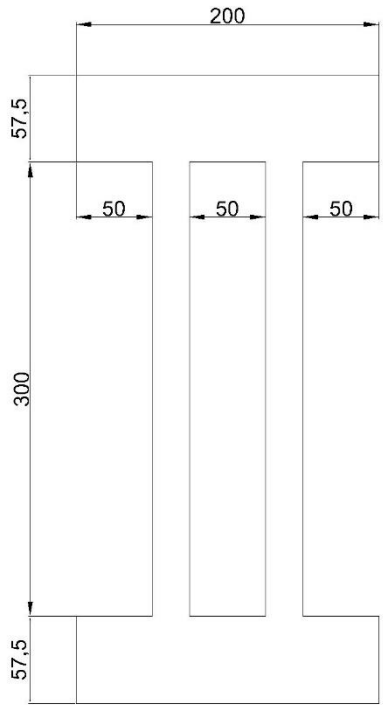

Figure 7. Cross Section of Metallic Elements

All of the materials except rebars were modelled by using C3D8R elements. This is a three dimensional, 8 noded element with reduced integration. The size of elements was selected as 50mm for frame and wall, 20mm for the metallic elements, and 10mm for polymer material. However, because the thickness of the polymer material in Abaqus is 15mm, the software used an element with sizes 10mm x 10mm x 7.5 mm for polymer material. The software modifies the mesh size when needed. The rebars of the frame were modelled using wire elements in the software. This kind of element is implemented for solid elements whose length is relatively much longer when compared with the dimensions of their cross sections. The rebars were embedded inside the concrete in software. That indicates that adherence between concrete and rebars was taken into account and the assembly can be assumed as reinforced concrete. For the analysis, explicit dynamic analysis was used. The frame was pushed up to 80mm lateral displacement in 8 seconds. By using the finite element method, Abaqus forms the system stiffness, mass, and damping matrices first. For the numerical solution of the equation of motion, in explicit analysis, the central difference method is used in Abaqus. In the central difference method, stiffness, mass, and damping matrices are not re-built in every step and the displacements at the step of I+1, are found by using the displacements at steps of I and I-1 (Demir, 2012). The equation of motion can be written as follows in the central difference method (Ramancharla):

$$\mathrm{m}\left[\frac{u_{i+1}-2u_i+u_{i-1}}{\Delta t^2}\right]+\mathrm{c}\left[\frac{u_{i+1}-u_{i-1}}{2\Delta t}\right]+ku_i=p_i \quad (4)$$

In Abaqus, in explicit dynamic analysis, the computational cost is low. A big power is not needed, most of the computational power is used for finding the internal forces of elements. If quasi-static analysis will be performed by using explicit dynamic analysis, the analysis must be performed under some circumstances. Because a static problem was transformed into a dynamic problem in such a case. If inertial forces were kept under a level, the problem can be assumed as static. To control this kinetic energy/total internal energy ratio must be controlled after the analysis. If this ratio is smaller than 0.10 then the analysis can be assumed to be quasi-static (Demir, 2012). The finite elements (mesh) of the system can be seen in Figure 8.

RESULTS AND DISCUSSION

Load Displacement Curves of First Group of Frames

In the first group of frames, two different types of walls and 10mm thick metallic elements were used. The frames were subjected to 80mm lateral displacement which indicates 0.026 lateral drift ratio. This ratio was selected because, for most of the buildings that were constructed after TSC 2007, 0.02 drift ratio was a limit value for the control of relative drift of one story according to others. The bare frame carried a 269632.53N maximum load. The initial stiffness of the bare frame can be considered as 21886.06 N/mm from the graph if the first point where linear elastic

behaviour is finished is taken into account. The initial stiffness of the frame with the first type of wall is nearly the same as the bare frame but it carried 435997.46N maximum load. However, if a second type of wall is used, the initial stiffness of the wall increases to 56198.27N/mm. This type of frame carried a 571437.7N maximum load. All

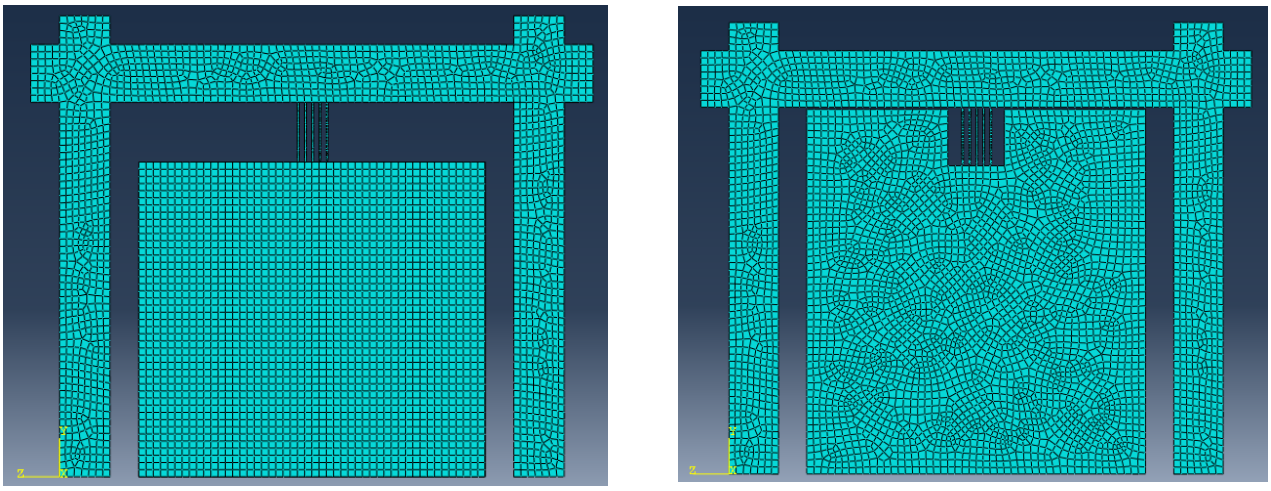

Figure 8. a. The Mesh of the Frame with 1st Type of Wall **b.** The Mesh of the Frame with 2nd Type of Wall

types of frames showed ductile behaviour until 0.026 drift ratio, however, the ductility of the frame with the second type of wall was the least one. The results of the bare frame were compared with the experimental and numerical study done before (Zhai et al., 2016). An acceptable discrepancy was seen between the results. In the previous study, according to experimental results, bare frame specimens carried 225000N maximum load. A small discrepancy can occur due to the differences in material class for concrete and rebar. Also in finite element modelling, factors like mesh size, element type, and analysis type can affect the results. The results of the previous study can be seen in Figure 9.

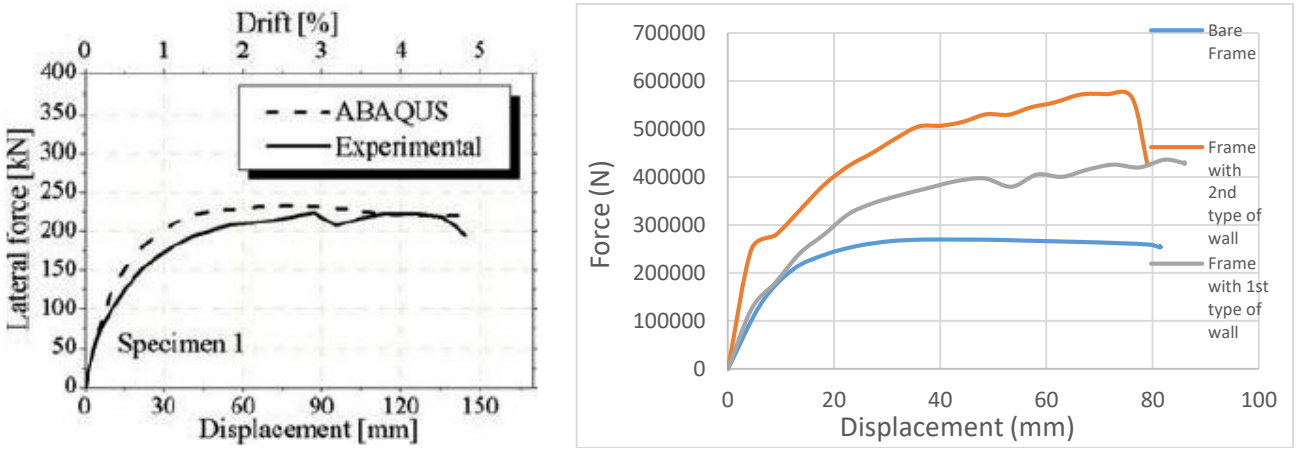

Figure 9. a. Force Displacement Curve of Bare Frame in Previous Study (Zhai et al., 2016) **b.** Force Displacement Curves of Frames with 10mm Thick Metallic Elements

Stress Analysis of the First Group of Frames

In Abaqus, equivalent Von Mises Stresses can be observed for materials after analysis. If von Mises stress exceeds the strength of material in a uniaxial stress situation, yielding of material is expected. Equivalent Von Mises stress can be written as the following equation if principal stresses exist only (Anonymous).

$$\boldsymbol{\sigma}_{eq} = \sqrt{\left[\left(\frac{1}{2}\right).(\sigma_1 - \sigma_2)^2 + (\sigma_2 - \sigma_3)^2 + (\sigma_3 - \sigma_1)^2\right]} \quad (5)$$

Also, for different components of frame assembly (wall, frame, metallic elements, etc.) the stresses can be seen separately in the menu in the software. In bare frame analysis, when the bare frame was pushed to 80 mm lateral displacement, in the concrete of the frame Mises stresses changed between values of 34.53MPa to 51.77MPa in damaged zones as seen in Figure 10. These values are already bigger than the strength of the material. This result is consistent with the results of the bare frame in the previous study where plastic hinges were formed at the column

ends and damage happened in the beam-column conjunction zone (Zhai et al., 2016). Because in beams in these zones, Mises stresses exceeded the tensile strength of the concrete material. As seen in Figure 11, in rebars Mises stresses exceeded the yield stress limit of steel material and reached the level of 517MPa maximum in plastic hinge zones. The results are consistent with previous study (Zhai et al., 2016).

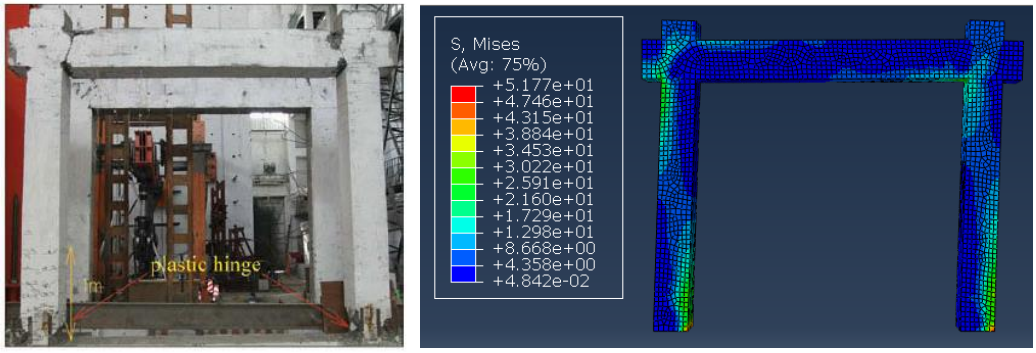

Figure 10. a. The Damage in Bare Frame in Previous Study (Zhai et al., 2016) **b.** The Mises Stress Distribution in Bare Frame

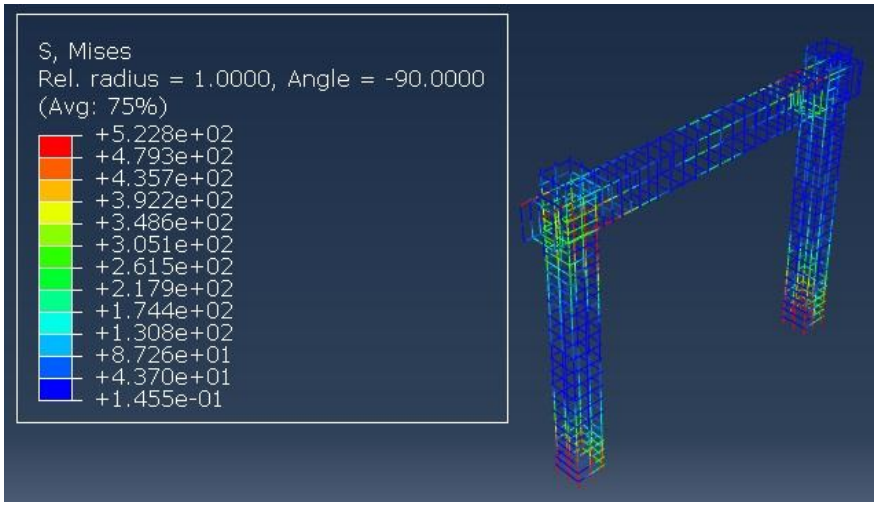

Figure 11. a. The Mises Stress Distribution in Rebars of Bare Frame

If Mises stresses in the walls of frames with first and second type of frame is observed, it can be concluded that damage can only be expected in a small region which is a conjunction joint of metallic elements and the wall. In this small region, Mises stresses varied between 15-22MPa for the first type of wall and 15-26 MPa for the second type of wall. However, in most of the walls, Mises Stresses were around 2-6.66 MPa. The results are seen in Figure 12.

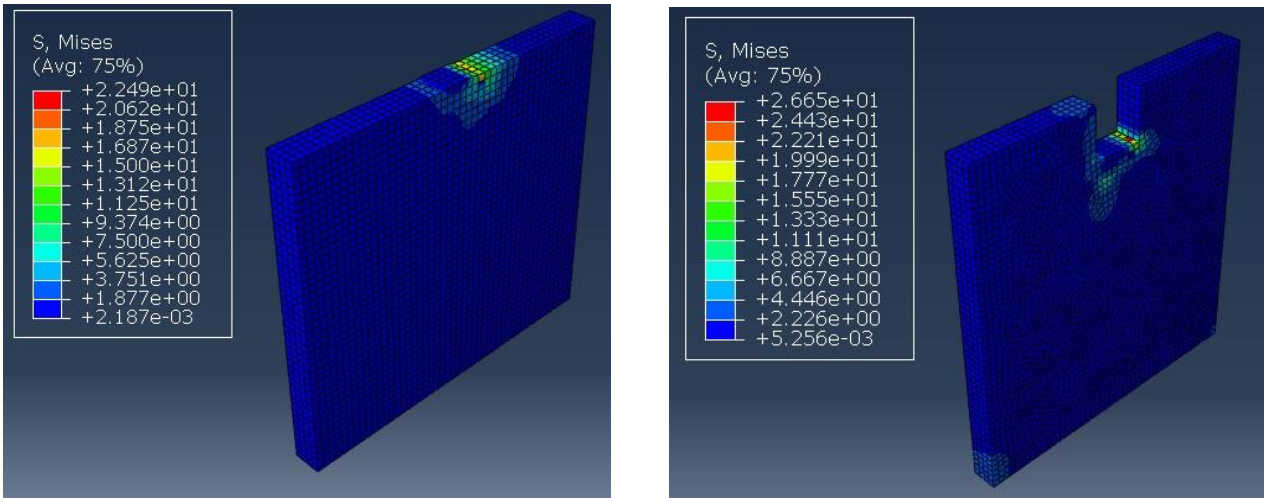

Figure 12. a. The Mises Stresses in 1st Type of Wall **b.** The Mises Stresses in 2nd Type of Wall

Observing max principal stresses shows that around the connection region between metallic elements and wall, max principal stresses are around 7.36MPa in 1st type of wall and around 6.86 MPa in 2nd type of wall as seen in Figure 13. Only in very small areas, it reaches 11.35-11.16MPa stress levels. From the stress analysis, it can be concluded that the 20cm thickness of the wall and the high strength of lightweight concrete material are capable of resisting the forces in most of the regions of the wall.

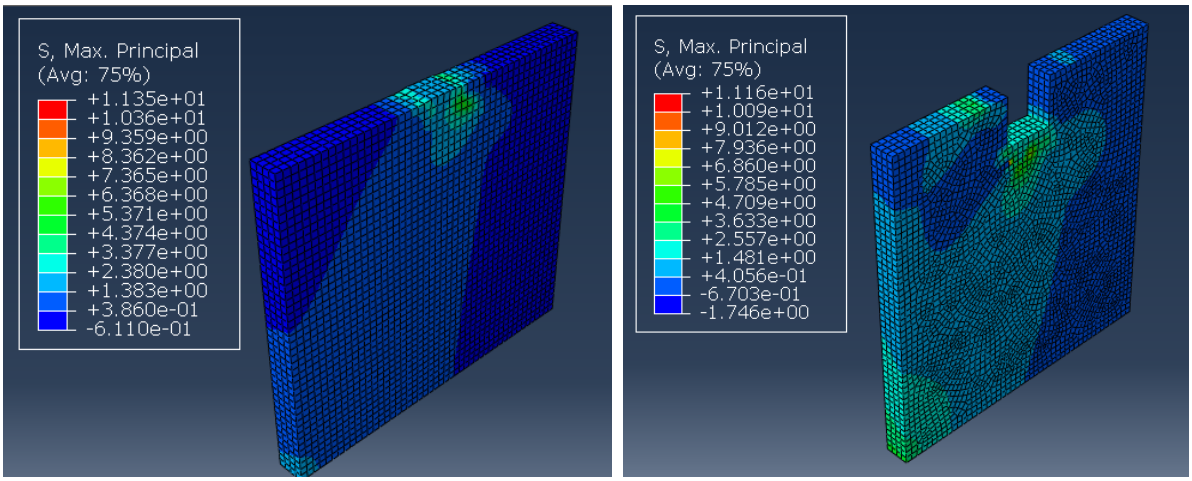

Figure 13. a. The Max. Principal Stresses in 1st Type of Wall **b.** The Max. Principal Stresses in 2nd Type of Wall

When the Mises Stresses in Metallic elements with 10cm is observed, both for the analysis with the first type of wall and for the analysis with the second type of wall, it is seen that in most of the regions of elements, the material has not reached the yield stress of the material (277 MPa). Only in conjunction joints with the elements and the RC Frame's beam, yielding has just started in metallic elements when the frame reached 80mm lateral displacement. For most of the regions, Mises stresses varied between 60 to 126 MPa in metallic elements in the case where the first type of wall is used and between 76 to 187 MPa in the metallic elements in the case where the second type of wall is used. The results can be seen in Figure 14. The average Mises stresses in the metallic elements with the second type of frame are higher than the average Mises stresses in the metallic elements with the first type of wall. The connection between the wall and frame in the second type causes an imaginary compressive strut behavior even though there is a gap between the wall and columns. Due to this, the stiffness of the frame increased, and behavior was changed as seen in Figure 9. Thus additional stresses affected the metallic elements and changed the Mises stress distribution in metallic elements in the frame with a second type of wall.

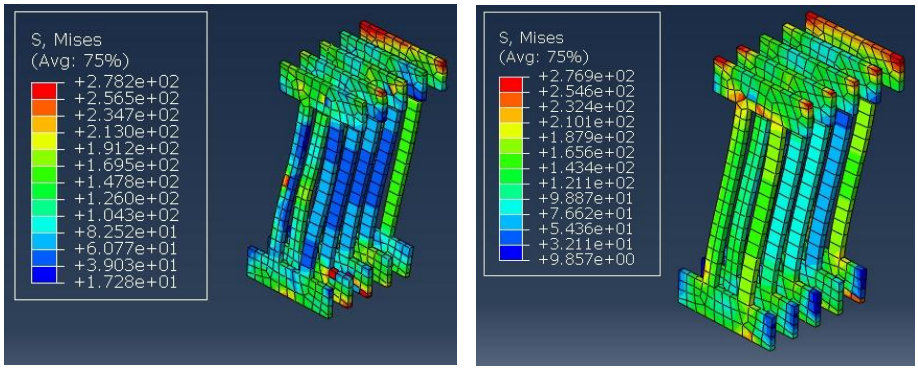

Figure 14. a. The Mises Stresses in Metallic Elements (10mm thick) with 1st Type of Wall b. The Mises Stresses in Metallic Elements (10mm thick) with 2nd Type of Wall

This type of strengthening increases the lateral rigidity of the frame. Also, by using less rigid steel elements, the yielding mechanism can be achieved and energy consumption can be achieved. For that purpose, analysis was renewed for the frame with 2nd type of wall, and elements with 5mm and 3mm thickness were implemented. The second type of wall is chosen for the analysis of less rigid elements in the light of the result analysis.

Load Displacement Curves of Second Group of Frames

In Figure 13, lateral load displacement values are given for frames with thinner metallic elements. The frame with 5mm thick elements carried a maximum load of 511kN when the displacement was 91.5mm, whereas the frame with 3mm thick elements carried 409.5kN when the lateral displacement was 71,5mm If the results are compared with the first group of analysis where 10mm thick elements were used, it can be seen that by increasing the thickness of metallic elements from 5mm to10mm, only 11,7% increase in lateral load capacity is achieved. The initial stiffness of a frame with 5mm thick elements is 61694.4N/mm, and the initial stiffness of a frame with 3mm thick elements is 29352.97 N/mm according to the point where linear elastic behaviour has been lost in Figure 15. The frames showed ductile behaviour.

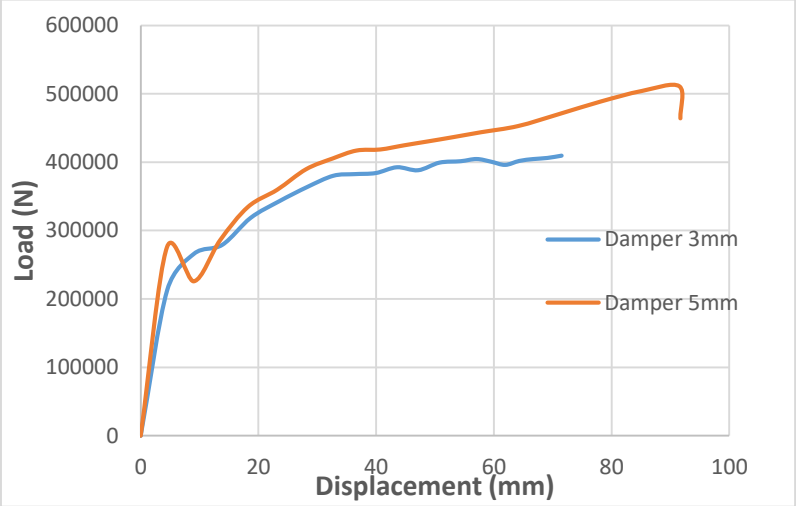

Figure 15. Load Displacement Curves of Frames with Second Type of Wall and Metallic Elements

The results of the proposed wall system can be compared with the results of the same frame with a traditional infill wall. The results taken from the previous experimental and numerical study are shown in Figure 16 (Zhai et al., 2016). If these results are compared in the best case, the proposed wall model in this study carried 72% more load than the traditionally infilled RC frame. In the worst case, the proposed wall with 3mm thick metallic elements carried 23% more load than the traditionally infilled frame. Even though some discrepancy is expected from bare frame comparison due to the differences in materials, still it can be concluded that the proposed wall is better than the traditional infill wall in terms of increasing lateral load capacity.

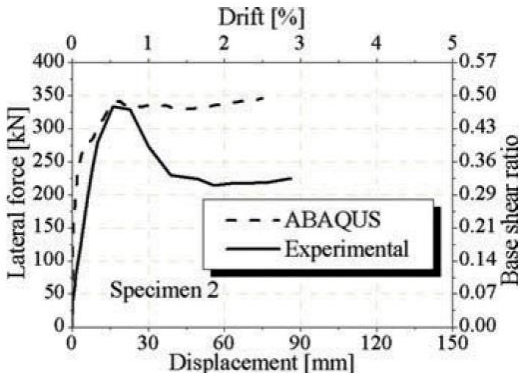

Figure 16. The Load-Displacement Curve of same RC Frame with Traditional Infill Wall from Previous Study (Zhai et al., 2016)

Stress Analysis of Metallic Elements in Second Group of Frames

If the Mises stress distribution in metallic elements is observed after the analysis, unlike the 10mm thick elements of group 1, it's seen that yielding occurred in the elements. Then the elements can be modelled as nonlinear elements in finite element based software for a more practical approach. Alternatively, instead of modelling the elements nonlinearly, an equivalent damping ratio can be calculated for the linear analysis of structures. The Mises Stresses can be observed in Figure 17.

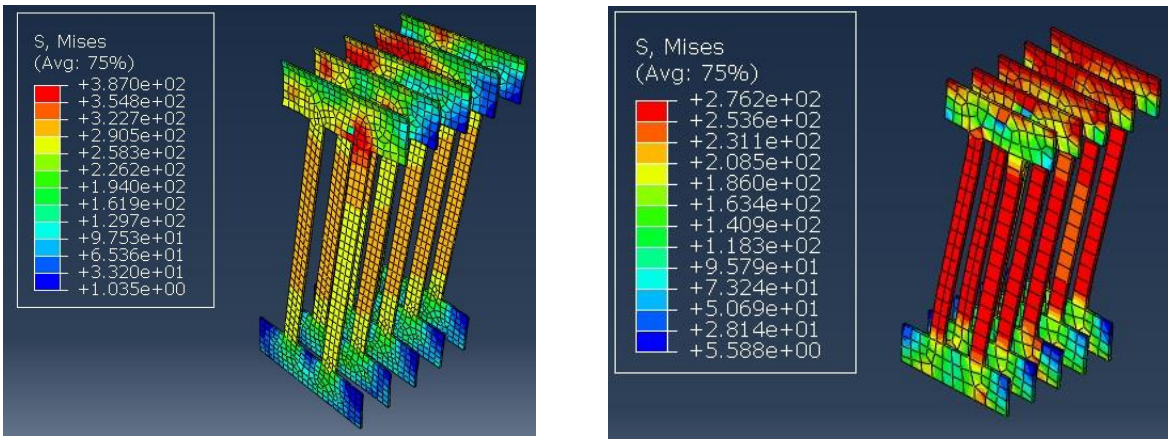

Figure 17. a. The Mises Stresses in 3mm Metallic Elements **b.** The Mises Stresses in 5mm Metallic Elements

Energy Ratios in the Frames

In Abaqus, dynamic explicit analysis was performed. In a previous study where a quasi-static loading of a historical wall was performed, the energy balance of the system in Abaqus was explained. Internal energy (E_I) (Total strain energy of the material), energy absorbed by viscous damping (E_v), kinetic energy of deforming material (E_{KE}), energy absorbed by frictional forces (E_{FD}), work done by external forces (E_W), and the total energy of the system can be written in the same equation as follows (Demir, 2012):

$$(E_I)+ (E_v)+ (E_{KE})+ (E_{FD})+ (E_W) = (E_I) \quad (6)$$

As stated earlier, in equation 6, "the kinetic energy of deforming material" / "total internal energy" ratio must be observed after analysis to check if the analysis can be accepted or not. In Abaqus after the analysis, the energy values for the whole model during the loading process can be seen. Typically, it is advisable to ensure that the kinetic energy does not surpass 5% to 10% of the internal energy during the majority of the process. As seen in Figure 18, throughout the loading, kinetic energy values are very low for the frame with 10mm panels and 2nd type of wall when compared with the total strain energy needed to push the frame. Also, for other frames, the ratio is checked and it's concluded that the analysis can be accepted as a quasi-static loading. In other words, the whole frame models were not accelerated enough to be accepted as a dynamic loading. So, the results can be compared with a quasi-static experiment.

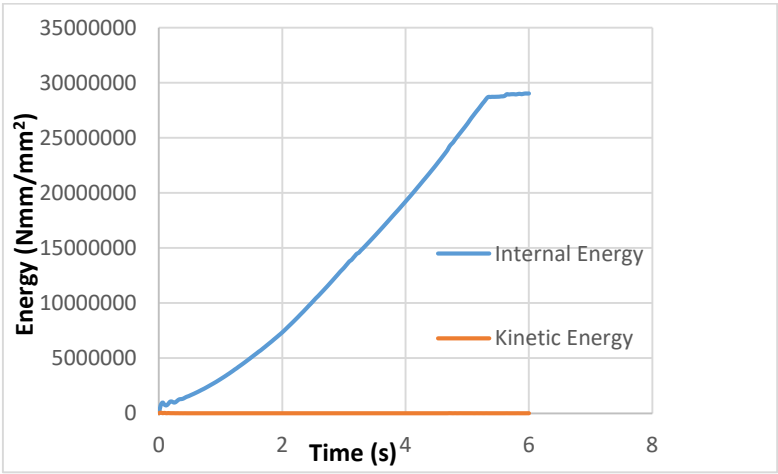

Figure 18. Internal Energy and Kinetic Energy of the Whole Frame

CONCLUSION

In this study, a practical wall system was proposed to improve the behaviour of RC frames. The results of the bare frame can be compared with a previous experimental study. In the previous study (Zhai et al., 2016) where the same dimensions of the RC frame were constructed with Chinese local steel and concrete materials, the bare frame carried 225kN load. The good agreement between the results of this study and the previous one shows that the results are trustable.

The first type of wall with 10mm metallic elements increased the lateral load carrying capacity of the frame from 269kN to 435kN. This indicates a 61% increase. If a second type of wall is used the interaction between wall and frame increases the lateral load capacity to 571kN. This indicates a 112% increase when compared with the bare frame, and a 31% increase with the analysis of the first type of wall. If 5mm thick metallic elements are used, the lateral load capacity increases to 511kN. This indicates a 10% decrease only if compared with the situation with 10mm thick elements. However, if 3mm thick elements are used with the second type of wall maximum load is 409.5kN which is 28% less than the strength of the frame with the second type of wall and 10mm thick elements. If these results are compared with the previous study (Zhai et al., 2016) where the RC frame is modelled with a traditional infill wall, in the best case, the proposed wall model in this study carried 72% more load than the traditionally infilled RC frame. In the worst case, the proposed wall with 3mm thick metallic elements carried 23% more load than the traditionally infilled frame.

The proposed wall increases the stiffness of the frame. The initial stiffness of the bare frame was 21886.06N/mm. If a second type of wall with 10mm thick elements is used, the initial stiffness of the frame increases to 56198.27N/mm which indicates a 156% increase. However, 3mm thick elements increase the stiffness only to 29352.97N/mm which indicates a 34% increase. The results show that different types of walls and metallic elements can be used for different design purposes.

In this study, it was observed that there was no serious damage at all in the lightweight concrete wall panel. Also, the usage of polymer material between the wall and beam in the second type of wall prevented local damage in the conjunction zone. This can be related to the fact that the high deformation ability of polymer material eliminates the stress concentrations as indicated by a previous study (Kwiecien, 2014). Unlike the 10mm thick elements of group 1, it's seen that yielding occurred in the elements with 5mm and 3mm thickness. Mises stresses reached around 354-387MPa in 3mm thick elements. This result indicates that thinner elements also can work as nonlinear yielding metallic dampers increasing the damping in the structure.

REFERENCES

Al-Shaikh, I., & Falah, N. (2014). Numerical analysis of masonry infilled RC frames, *Journal of Science and Technology*, 19:2. https://doi.org/10.20428/jst.v19i2.772

Abdulla, K., F., Cunningham, L., S., & Gillie, M. (2017). Simulating masonry behaviour using a simplified micro model approach. *Engineering Structures*, 151, 349-365

Bai, J., & Ou, J., (2012, September). Plastic limit state design of frame structures based on the strong column weak beam failure mechanism. In 2012 15th World Conference on Earthquake Engineering. WCEE

Demir, C. (2012). Seismic Behaviour of Historical stone masonry. Phd Thesis. Istanbul Technical University Civil Engineering.

Dassault Systems Simula ABAQUS, Modelling fracture and Failure, Lecture 6

Gao, J., Sun, W., & Morino, K. (1997). Mechanical properties of steel fiber-reinforced high-strength lightweight concrete. *Cement and Concrete Composites*, 19, 307-313. https://doi.org/10.1016/S0958-9465(97)00023-1

Inculet, V. (2016) Nonlinear analysis of earthquake induced vibrations. Master Thesis. Aalborg University School of Engineering and Science, 79s.

Kuruşçu, A., O. (2012) Yığma duvar ve temellerde doğrusal olmayan modelleme. Doktora Tezi. Yıldız Teknik Üniversitesi Fen Bilimleri Enstitüsü İnşaat Mühendisliği Anabilimdalı, 171 s.

Kwiecien, A. (2014). Shear bond of composites to brick applied highy deformable in relation to resin epoxy interface materials. *Materials and Structures*, 47, 2005-2020, https://doi.org/10.1617/s11527-014-0363-y

Ksiel, P. (2018). Model approach for polymer flexible joints in precast elements joints for concrete pavements. Phd Thesis. Krakow University of Technology Civil Engineering.

Koman, H. (2021). Harçsız bloklar kullanılarak yapıların deprem davranışının iyileştirilmesi. Doktora Tezi. Manisa Celal Bayar Üniversitesi Fen Bilimleri Enstitüsü İnşaat Mühendisliği Anabilim Dalı, Manisa 142s.

Kahramanmaraş Depremlerine ait ön değerlendirme raporu. (2023). https://insaatmuh.mcbu.edu.tr/ Accessed 12.06.23.

Li, H., Li, G., & Wang, S. (2014, July). Study and Application of Metallic Yielding Energy Dissipation Devices in Buildings. In 10th National Conference on Earthquake Engineering (pp. 21-25).

Lin, K., Totoev, Y.Z., Liu, H., & Guo,T. (2016). In plane behaviour of a reinforcement concrete frame with a dry stack masonry panel, *Mdpi Materials*, 9, 108. https://doi.org/10.3390/ma9020108

Nikam, S., Wagholikar, S., & Patil, G., (2014). Seismic energy dissipation of a building using friction damper. *International Journal of Innovative Technology and Exploring Engineering*, 10, 2278-3075.

Naeem, A., Lee, M., & Kim, J., (2015, April) Steel Honeycomp Dampers for Seismic Retrofit of Structures. In 2015 International Conference on Environment and Civil Engineering.

Obaidat, Y., T. (2011) Structural retrofitting of concrete beams using FRP. Phd Thesis. Lund University Civil Engineering.

Ramancharla, P., K. Nptel Online Course, Indian Institute of Technology, Madras, India

Viskovic, A., Zuccarino, L., Kwiecien, A., Zajac, B., & Gams, M. (2017) Quick seismic protection of weak masonry infilling in filled frame structures using flexible joints. *Key Engineering Materials*, 747, 628-637, https://doi.org/10.4028/www.scientific.net/KEM.747.628

Yıldırım, S., Aşık, G., Erkuş, B., Yetimoğlu, Y., Tonguç, Y., & Mualla, I., (2014 Ağustos). Retrofit of a reinforced concrete building with friction dampers. In Second European Conference on Earthquake Engineering And Seismology, (pp. 25-29).

Zhai C., Kong, J., Wang, X., & Chen, Z., (2016). Experimental and finite element analytical investigation of seismic behavior of full-scale masonry infilled RC frames, *Journal of Earthquake Engineering*, 20:7, 1171-1198. https://doi.org/10.1080/13632469.2016.1138171